Topological Edge States in Quasiperiodic Locally Resonant Metastructures

Yiwei Xia, Alper Erturk, and Massimo Ruzzene

Phys. Rev. Applied **13**, 014023 — Published 14 January 2020

DOI: 10.1103/PhysRevApplied.13.014023

Topological edge states in quasiperiodic locally resonant metastructures

Yiwei Xia,[1,*] Alper Erturk,[1] and Massimo Ruzzene[2]

[1] *George W. Woodruff School of Mechanical Engineering, Georgia Institute of Technology, Atlanta, 30332, USA*

[2] *Department of Mechanical Engineering, University of Colorado Boulder, 80309, USA*

(Dated: December 20, 2019)

We investigate the dynamic behavior and topology of quasiperiodic resonant metastructures. We show that the quasiperiodic arrangement of resonators introduces frequency bandgaps in addition to the locally resonant bandgap defined by the natural frequency of the resonators. The concept is illustrated on a beam with an array of mechanical resonators. Numerical evaluation of the spectrum as a function of the quasiperiodic arrangement of resonators reveals a structure reminiscent of a Hofstadter butterfly and allows the study of key topological properties. Results illustrate the occurrence of additional bandgaps that are topologically non-trivial and that host edge localized modes in finite structures. The occurrence of these gaps and of the associated edge states is demonstrated experimentally by measuring the frequency response of the beam and by evaluating the spatial distribution of selected operational deflection shapes. The results unveil the potential of deterministic quasiperiodic structural designs to induce wave localization and attenuation over multiple frequency bands, which may find applications in vibration isolation and energy harvesting, among others.

I. INTRODUCTION

Locally resonant (LR) metamaterials and metastructures have been broadly investigated in the past decades. Theoretical and numerical studies have shown that linear local resonators produce sub-wavelength frequency bandgaps which enable low frequency attenuation of sound and vibrations [1–7]. Most investigations have considered nominally identical resonators that are regularly, or periodically, placed within the structure. In these cases, the LR bandgap center frequency is defined through the natural frequency of the resonators, while its width is mostly determined by the added inertia [7]. Attempts at extending the resonant gap through non-uniform resonators, both in terms of their natural frequency and of their spacing, can be found in [3, 8, 9], among others. Parallel to these efforts, there is considerable interest on the conditions that govern the onset of localization [10–12]. Vibration localization can be both beneficial in terms of isolating components and limiting exposure, but can also be the source of catastrophic failures [13], and therefore is of great relevance to the engineering community.

Inspired by the discovery of topologically non-trivial phases in electronic [14] and photonic [15] systems, various classes of topological phenomena such as quantum Hall and quantum spin Hall effects have been studied and realized in acoustic and mechanical systems [16]. These works exploit defect-immune modes localized at edges or interfaces for robust acoustic/elastic waveguiding. Recently, topological phases have also been explored in lower physical dimensional systems by exploiting virtual dimensions in relevant parameter spaces [17–20]. In particular, quasi-crystalline or quasiperiodic structures have been linked to topological insulators [21–23]. Quasiperiodicity defines a broad class of geometrical patterns, of which periodic assemblies are particular cases. Thus, the study of quasiperiodic (QP) arrangements of inclusions can extend the range of capabilities of periodic metamaterials and metastructures [24].

A recent line of work considers a framework to investigate QP systems based on the evaluation of their spectral properties, the evaluation of the density of states, and the estimation of topological invariants that may characterize non-trivial gaps and the onset of associated edge states [25–28]. For example, recent work in mechanics [25] has demonstrated that topological boundary modes can emerge solely from the patterning of a metamaterial, in a manner that is entirely independent upon the structure of the resonators and their coupling. The experimental observations in [25] also show the onset of localized modes at the boundary of finite arrays of discrete mechanical resonators, implemented in the form of a chain of magnetically-coupled spinners. Topological boundary and interface modes in QP acoustic waveguides are also observed in [26], while reconfigurable QP acoustic crystals [27] are employed to experimentally observe their spectrum in the form of a Hofstadter butterfly [29]. Furthermore, the numerical results in [28] have shown how an Hofstadter spectrum also characterizes continuous structural beams supported by a QP array of ground springs, and how localized modes can be predicted through topological considerations on such spectrum. The studies referenced above provide insights into modes that are localized at edges or interfaces and suggest new methodologies for wave transport and localization. Also, this body of work generally contributes to the literature that regards QP geometries as projections of higher dimensional manifolds onto lower dimensional lattices, and that explores topological properties of higher dimensional periodic systems, to assess properties in the lower dimensional physical space.

* yxia63@gatech.edu

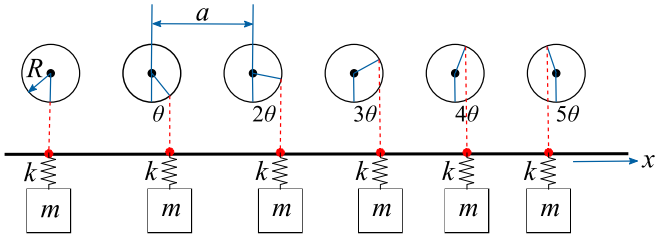

FIG. 1. Projection operation for placement of the local resonators according to the procedure described in [25]).

II. QUASIPERIODIC PATTERN GENERATION

Motivated by previous contributions, we here investigate a LR beam with QP distributions of resonators. Extending the results in [28], we consider elastic beams in transverse motion equipped with local resonators located at positions defined by the projection operation described in [25]. This pattern-generating procedure identifies families of structures ranging from periodic to QP obtained through smooth variation of the parameters defining the projection, which can be interpreted geometrically as shown in Fig. 1. Accordingly, the location of resonator s is given by:

$$x_s = sa + R\sin(2\pi s\theta) \tag{1}$$

Here, a is the distance between the centers of adjacent circles defining the spacing between resonators in an underlying periodic arrangement, while the radius of the circle $R < a/2$ and the angular increment θ define the projection. Rational and irrational θ values define periodic and QP patterns respectively. For $\theta = 0$, the system has periodicity of a and the resonators are placed uniformly on the beam. For rational $\theta = p/q$ (p and q are coprime integers), the system has periodicity of qa. In contrast, no periodicity or translational symmetry exists for irrational θ values. In addition, all resonators are here assumed to have the same mass m and stiffness k. The governing equations for the beam and the s-th resonator are:

$$D\frac{\partial^4 w(x,t)}{\partial x^4} + \rho A\frac{\partial^2 w(x,t)}{\partial t^2} - k\sum_s w_s(t)\delta(x-x_s) = 0 \tag{2}$$

$$m\frac{\partial^2 (w(x_s,t)+w_s(t))}{\partial t^2} + kw_s(t) = 0 \tag{3}$$

where $w(x,t)$ is the transverse displacement of the beam and $w_s(t)$ is the displacement of the s-th resonator relative to the beam. Also, $D = EI$ is the beam bending stiffness, where E is the Young's modulus, and I is the second moment of area of the beam cross section, while ρ is the density and A is the cross-sectional area. We consider an aluminum beam (mass density $\rho = 2700$ kg/m^3, Young's modulus $E = 69$ GPa) of cross section 0.8×25.2 mm^2. All resonators have a natural frequency of 90 Hz, and the added mass ratio is 1.26. The added mass ratio here is defined as the ratio of total mass of added resonators to the mass of the plain beam without resonators. In addition, $a = 5.08$ cm and $R = 0.3a$ are chosen as fixed dimensions in accordance with the considered experimental setup described below.

III. TOPOLOGICAL BANDGAPS AND EDGE-LOCALIZED STATES

The study is conducted in terms of variations in θ, which is the considered free, QP parameter. We first evaluate the spectrum of an infinite beam, which is approximated by considering all rational values of θ that are commensurate with $S = 600$ cells. Periodic boundary conditions are imposed on both ends of the beam, so that it geometrically resembles a ring (refer to [28] for details). Employing an analysis approach based on Galerkin's approximation [28], we evaluate the resonant frequencies for all configurations ($\theta = s/S, s = 1, 2, \ldots, S$), and plot them to obtain the approximated bulk spectrum shown in black in Fig. 2a. The resonant frequencies of the ring discretize the bulk spectrum. The density of the discretization increases as the number of unit cells S increases. Variation of vibrational frequencies in terms of QP parameter leads to a pattern that is reminiscent the Hofstadter Butterfly [29]. In addition, estimating the spectral properties of a finite, simply supported beam of length, $L = aS$, including $S = 30$ unit cells leads to the finite structure frequencies, denoted by the red dots in Fig. 2a. Both bulk and finite spectra are characterized by a LR bandgap that is topologically trivial, as demonstrated by the fact that it remains constant as θ varies. Depending on the boundary conditions of the finite structure, the modes localized at the edge may or may not appear inside the LR bandgap. This gap separates two spectral regions, which feature several additional bandgaps whose center frequencies and widths depend on the value of θ. These additional gaps, topologically non-trivial, are crossed by several modes of the finite structure, whose distinctive feature is their localized nature.

The zoomed-in spectrum of Fig. 2b compares selected modes corresponding respectively to bulk and finite structure frequencies. Notably, the modes in the finite beam that appear in the bandgap are edge-localized at the right boundary ($x = L$). Also, the response of the resonators (shown in red circles) is of a localized nature when the beam's deflection is localized, while the relative displacements of the resonators are in phase and out of phase with respect to the beam at frequencies below and above the LR bandgap, respectively. The fact that all of the modes spanning the non-trivial gaps are localized at the right boundary is a consequence of the way the finite beam is constructed from the pattern defined previously in Eq. (1). All finite beams are constructed by placing the first resonator at the space location at $x = a + Rsin(2\pi\theta)$ and adding resonators to the right boundary.

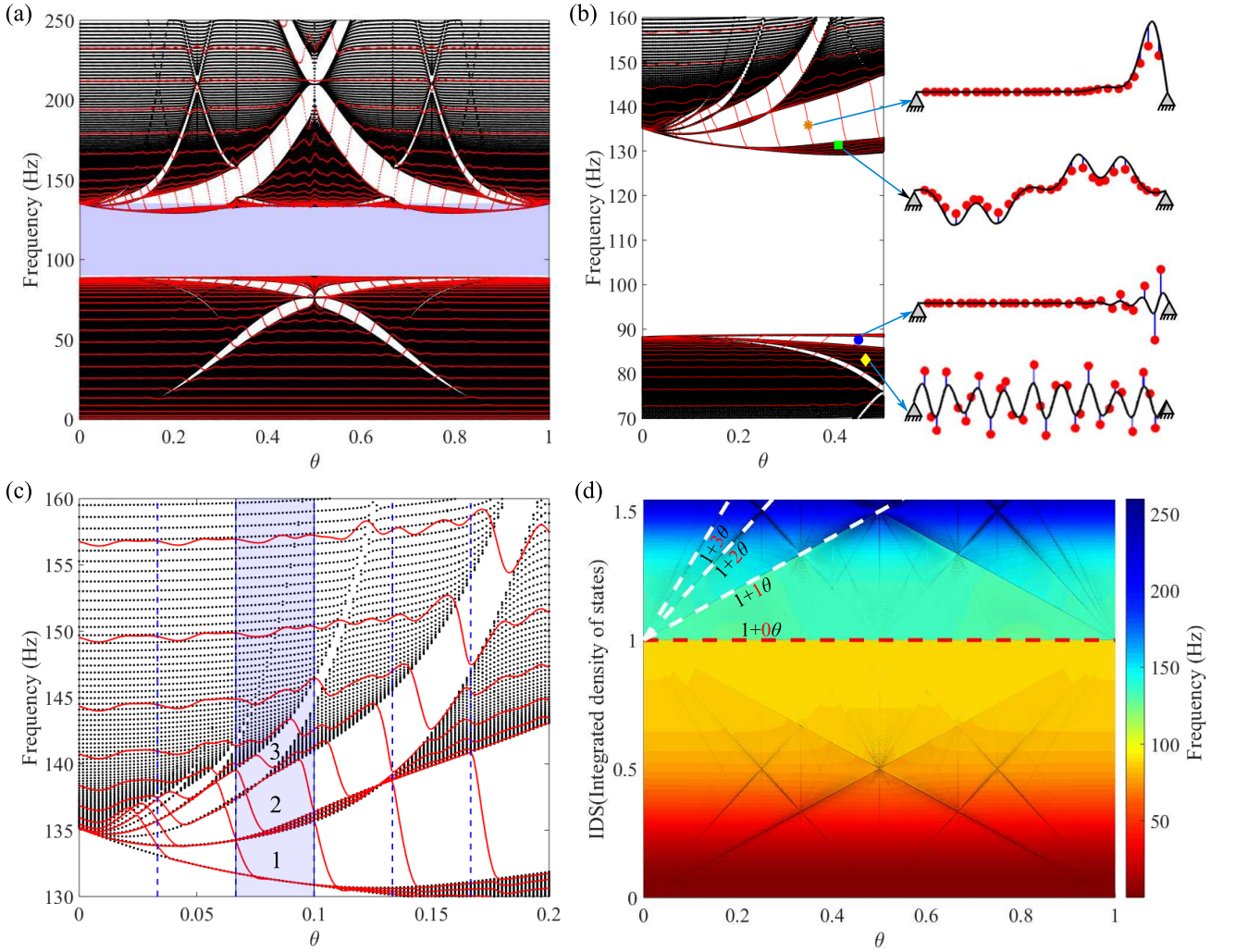

FIG. 2. (a) Bulk (black) and finite beam (red) spectra as a function of θ. The finite beam spectrum, obtained for a finite, simply supported beams with 30 resonators, shows the presence of modes spanning the non-trivial gaps. The blue shaded area highlights the LR bandgap, which is estimated according to the formula derived in [7]. (b) Detail of the spectrum showing four frequencies and corresponding bulk and edge-localized modes (the black curve represents the deflection of the beam, while the red circles denote the displacements of the resonators). (c) Detail of spectrum showing three labeled non-trivial topological bandgaps with increasing number of topological modes (blue dashed lines separate regions between commensurate values of θ, while the blue shaded area highlights the region between $\theta = 2/30$ and $\theta = 3/30$). (d) IDS as a function of θ exhibits sharp linear jumps at the bandgaps. The slope of three of these lines (highlighted by the white dashed lines, and corresponding to the three gaps labeled in (c)), is equal to $m = 1, 2, 3$, while for the LR bandgap (highlighted by the red dashed line) is $m = 0$, which indicates that this band is topologically trivial.

The existence of edge states can be predicted through the analysis of the topological properties of the bands, which are conveniently uncovered by estimating the Integrated Density of States (IDS) for the system [25, 28]. Non-trivial gaps and the resulting onset of edge states spanning them are associated to changes in the IDS as θ varies. In the IDS representation of Fig. 2d, a bandgap appears as a line, whose slope m indicates the number of topological boundary modes that span the bandgap in the interval between two subsequent commensurate values of θ [28]. In this case, three IDS lines corresponding to the three topological bandgaps (labeled in Fig. 2c) are shown as white dashed lines in Fig. 2d, whereby $m = 1, 2, 3$ respectively is the slope of the corresponding gaps. The red dashed IDS line related to the LR bandgap has a slope of $m = 0$, which indicates its topologically trivial nature and the lack of associated edge states spanning the gap (see Fig. 2a).

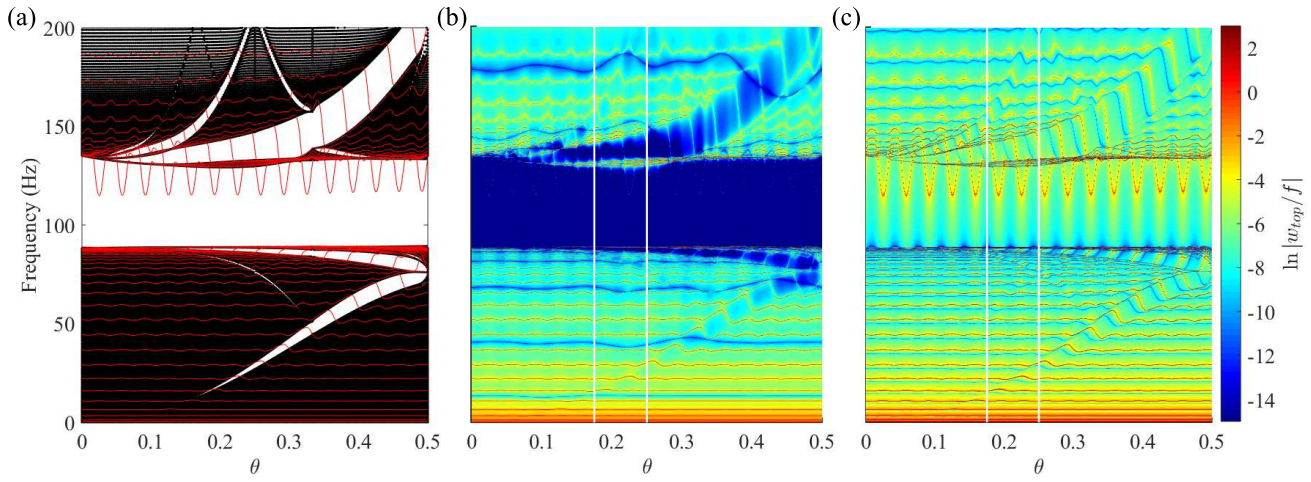

FIG. 3. (a) Bulk spectrum (black) and finite spectrum for a clamped-free beam with 30 resonators (red). (b) Numerical frequency response function of the beam spatially averaged between 20% and 30% of the beam span: the color map evolving from blue to red corresponds to the log scale of the magnitude. The blue regions highlight the low response ranges corresponding to the bandgaps. (c) Numerical frequency response function of the beam spatially averaged between 90% and 100% of the beam span: the response near the beam tip highlights the presence of resonances within the gaps which correspond to edge states. Vertical white lines in (b,c) correspond to the values of $\theta = 0.175$ and $\theta = 0.25$ considered in the experiments.

IV. NUMERICAL ANALYSES: A CANTILEVER BEAM

The finite system is implemented as a cantilever beam with clamped-free boundary conditions, with excitation applied at the free end. Numerical analyses (Fig. 3) are performed to evaluate the presence of the LR bandgap and of additional gaps, and to guide the selection of θ values for experimental investigation. On the finite structure, bandgaps are conveniently visualized by evaluating the frequency response function for the beam, averaged over portion of the length. The choice of the portion of the beam to be averaged is driven by the need to show the response far from the excitation and not too close to the clamped boundary, so that the LR bandgap together with other additional topological bandgaps is visible in the averaged frequency response. For example, Fig. 3b shows frequency response, corresponding to the ratio of magnitude of beam transverse deflection (output) to magnitude of input (forcing), averaged between 20%-30% of the span from the clamped end. As a result, the color map in Fig. 3b is characterized by low response regions (in blue) that highlight the attenuation occurring in the bandgaps. This representation clearly outlines both the LR bandgap and the additional topological gaps as θ varies. In contrast, Fig. 3c, obtained by averaging the beams response near the excitation, i.e. between 90%-100% of the span, clearly highlights the modes of the finite systems, including the resonances localized in the gaps associated with the finite system. Of these modes, those in the LR gap are not topological, and solely depend on the considered types of boundary conditions. Compared with the spectrum of the finite beam with simply-supported boundaries on both ends (Fig. 2a), the spectrum of the clamped-free beam (Fig. 3a) has defect modes inside the trivial LR bandgap. The non-trivial additional gaps are instead spanned by resonant modes as θ varies regardless of the boundary conditions.

V. EXPERIMENTAL INVESTIGATIONS

For the experiments, $\theta = 0.175$ and $\theta = 0.25$ ensure a well defined separation between the modes associated with the LR gap and the additional bandgap. The selected two cases are highlighted in white lines in Fig. 3b and Fig. 3c for reference. The experimental investigations are presented to confirm the existence of the topologically non-trivial bandgaps and the occurrence of edge-localized modes.

The finite system is physically implemented by employing a 1.524 m long aluminum cantilever beam with 30 resonators (Fig. 4). Each resonator consists of a 8.26 cm long strip of spring steel, which is 0.5 mm thick and 6.35 mm wide. Each strip is clamped symmetrically along the beam, thus forming two identical cantilevers. Two 6.35 mm^3 permanent magnets are placed at the tip of each cantilever, to add a tip mass of 3.6 g. The resulting natural frequency of each resonator is measured to be around 90 Hz. The beam is clamped vertically on one end, and is excited by an electrodynamic shaker at the free end (Fig. 4c). The force applied by the shaker is recorded by a force transducer, while the beam's velocity field is mapped by a scanning laser Doppler vibrometer (SLDV) over a grid of 158 points along the beam length (from the clamped boundary at top, $x = 0$, to the free end at bottom, $x = L$), which corresponds to a spatial resolution of 9.65 mm.

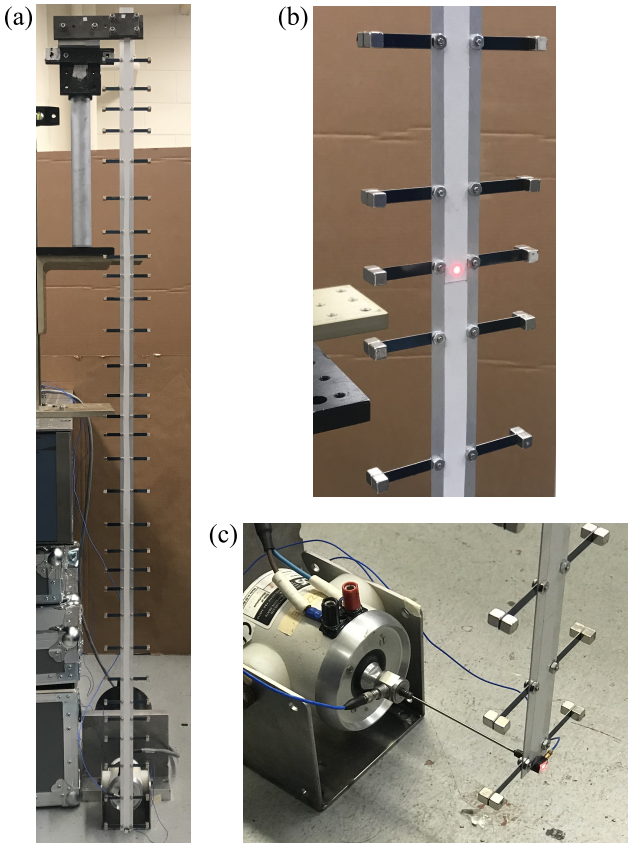

FIG. 4. Experimental setup: cantilever beam with 30 resonators. (a) Front view of the beam, (b) close-up of the resonators, and (c) view of the tip of the beam, excited by a electrodynamics shaker.

Experimental frequency response of the beam and measured spatial distributions of selected operational deflection shapes are shown in Fig. 5b-d for $\theta = 0.175$ and in Fig. 5f-g for $\theta = 0.25$. The spatial distributions are normalized with respect to the displacements at the free end, $w(L)$. The LR bandgap and the topological bandgap are clearly observed from on the measured frequency response averaged between 20% and 30% of the beam span, ie. away from the excitation location. Overall, the frequency location and frequency width of these bands agree well with the theoretical predictions shown as green and red shaded areas in Fig. 5b and 5f. Both center frequency and width of the topological bandgap increase as the QP pattern parameter θ varies from 0.175 to 0.25, which also agrees with the theoretical trend. Furthermore, the measured frequency response average near the free end, i.e. between 90% and 100% of the beam span, shows the presence of the localized modes which correspond to response peaks within the gap highlighted in Fig. 5c and 5g. As expected from theoretical predictions, the measured localized mode (red circle) for each case appears within the topological bandgap, and the localized nature at the edge is well confirmed by the corresponding operational deflection shape plotted in red, and labeled 'II' in Fig. 5d and 5h. In addition, for each θ value considered, 3 bulk, non-localized modes are also presented to illustrate their global deflection patterns. These modes are labeled 'I', 'III' and 'IV' in the figure, and their corresponding frequencies are part of the bulk spectrum, respectively in the frequency range before the LR bandgap, between the LR and topological bandgap, and after the topological bandgap. To be noticed, unlike the cluster of several modes between LR bandgap and the above additional non-trivial bandgap shown in the simulations (Fig. 3b), experimental measurements capture one distinguishable mode III (blue square), which can be due to the damping effect. The measured deflection shape of the beam at mode III has deflections at both the free end and close to the clamped boundary, confirming itself as a bulk mode.

VI. CONCLUSIONS

In conclusion, we investigated locally resonant metastructures in the form of beams with QP distributions of resonators. By varying the parameter θ defining the locations of the resonators, additional non-trivial topological bandgaps are created. In finite metastructures, these bands host modes that are localized at the boundary and whose frequency can be chosen through proper selection of the QP parameter defining the location of the resonators. The onset of the LR bandgap, and of the additional non-trivial bandgaps with associated edge states is demonstrated through numerical simulations, and in experiments conducted on a cantilever beam carrying an array of 30 resonators. The findings of the study suggest the application of QP placement of resonators, or in general of mechanical inclusions, as a potentially effective way to achieve vibration attenuation over multiple sub-wavelength frequency bands. In addition, the ability to induce vibration localization at frequencies defined by the placement of resonating inclusions may find applications in vibration isolation and energy harvesting.

ACKNOWLEDGMENTS

The authors acknowledge the funding support from the National Science Foundation through EFRI 1741685 grant and Army Research Office through grant W911NF-18-1-0036.

[1] Z. Liu, X. Zhang, Y. Mao, Y. Zhu, Z. Yang, C. T. Chan, and P. Sheng, Locally resonant sonic materials, Science **289**, 1734 (2000).

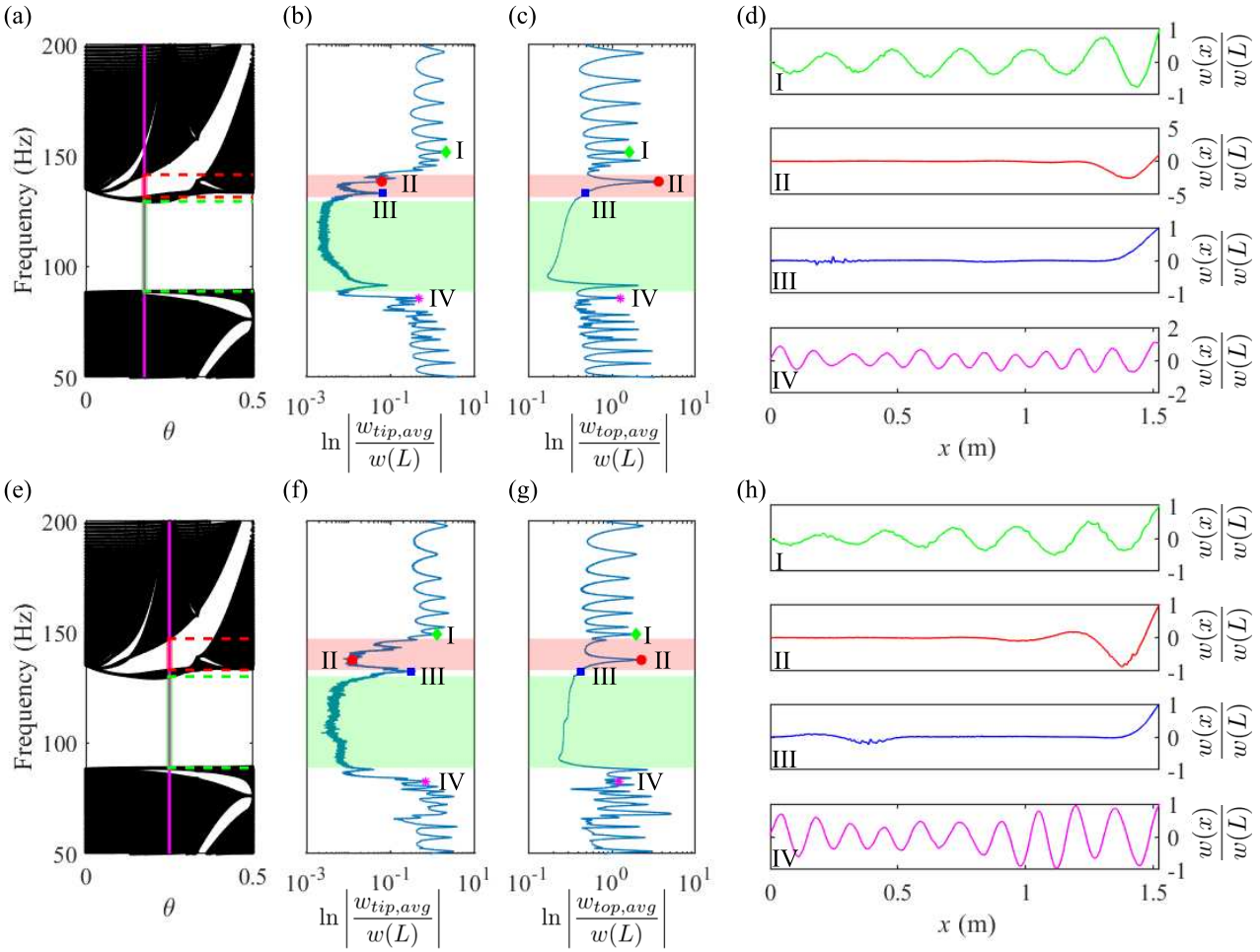

FIG. 5. (a,e) Detail of numerical bulk spectrum with vertical magenta lines corresponding to $\theta = 0.175$ and $\theta = 0.25$. The green and red dash lines show the theoretical boundaries of the LR and non-trivial topological bandgaps respectively. (b-d) Experimental results for $\theta = 0.175$. (f-h) Experimental results for $\theta = 0.25$. Magnitude of beam frequency response spatially averaged between 20% and 30% (b,f), and between 90% and 100% (c,g) of beam span. Green and red shaded areas highlight the theoretical LR and topological bandgaps. (d,h) Measured deflection shapes of the beam. Modes 'I', 'III' and 'IV' are bulk modes at frequencies respectively before the LR gap, between the LR and topological bandgap, and after the topological bandgap. The corresponding frequencies are marked by the green diamond, blue square and magenta asterisk in (b,c,f,g). The mode labeled as 'II' in (d,h) is edge-localized, and its frequency falls in the topologically non-trivial gap, and it is marked by red circle in (c,g).

[2] D. Yu, Y. Liu, H. Zhao, G. Wang, and J. Qiu, Flexural vibration band gaps in euler-bernoulli beams with locally resonant structures with two degrees of freedom, Physical Review B **73**, 064301 (2006).

[3] H. Sun, X. Du, and P. F. Pai, Theory of metamaterial beams for broadband vibration absorption, Journal of Intelligent Material Systems and Structures **21**, 1085 (2010).

[4] M. Oudich, M. Senesi, M. B. Assouar, M. Ruzenne, J.-H. Sun, B. Vincent, Z. Hou, and T.-T. Wu, Experimental evidence of locally resonant sonic band gap in two-dimensional phononic stubbed plates, Physical Review B **84**, 165136 (2011).

[5] M. B. Assouar, M. Senesi, M. Oudich, M. Ruzzene, and Z. Hou, Broadband plate-type acoustic metamaterial for low-frequency sound attenuation, Applied Physics Letters **101**, 173505 (2012).

[6] R. Zhu, X. Liu, G. Hu, C. Sun, and G. Huang, A chiral elastic metamaterial beam for broadband vibration suppression, Journal of Sound and Vibration **333**, 2759 (2014).

[7] C. Sugino, S. Leadenham, M. Ruzzene, and A. Erturk, On the mechanism of bandgap formation in locally resonant finite elastic metamaterials, Journal of Applied Physics **120**, 134501 (2016).

[8] D. Cardella, P. Celli, and S. Gonella, Manipulating waves by distilling frequencies: a tunable shunt-enabled rainbow trap, Smart Materials and Structures **25**, 085017 (2016).

[9] P. Celli, B. Yousefzadeh, C. Daraio, and S. Gonella, Bandgap widening by disorder in rainbow metamaterials, Applied Physics Letters **114**, 091903 (2019).

[10] C. Hodges, Confinement of vibration by structural irregularity, Journal of Sound and Vibration **82**, 411 (1982).

[11] C. Hodges and J. Woodhouse, Vibration isolation from irregularity in a nearly periodic structure: theory and measurements, The Journal of the Acoustical Society of America **74**, 894 (1983).

[12] D. M. Photiadis and B. H. Houston, Anderson localization of vibration on a framed cylindrical shell, The Journal of the Acoustical Society of America **106**, 1377 (1999).

[13] C. Pierre and E. Dowell, Localization of vibrations by structural irregularity, Journal of Sound and Vibration **114**, 549 (1987).

[14] M. Z. Hasan and C. L. Kane, Colloquium: topological insulators, Reviews of modern physics **82**, 3045 (2010).

[15] L. Lu, J. D. Joannopoulos, and M. Soljačić, Topological photonics, Nature photonics **8**, 821 (2014).

[16] G. Ma, M. Xiao, and C. Chan, Topological phases in acoustic and mechanical systems, Nature Reviews Physics **1**, 281 (2019).

[17] Y. Kraus, Y. Lahini, Z. Ringel, M. Verbin, and O. Zilberberg, Topological states and adiabatic pumping in quasicrystals, Physical Review Letters **109**, 106402 (2012).

[18] Y. Kraus and O. Zilberberg, Quasiperiodicity and topology transcend dimensions, Nature Physics **12**, 624 (2016).

[19] K. Madsen, E. Bergholtz, and P. Brouwer, Topological equivalence of crystal and quasicrystal band structures, Physical Review B **88**, 125118 (2013).

[20] T. Ozawa, H. M. Price, N. Goldman, O. Zilberberg, and I. Carusotto, Synthetic dimensions in integrated photonics: From optical isolation to four-dimensional quantum hall physics, Physical Review A **93**, 043827 (2016).

[21] D.-T. Tran, A. Dauphin, N. Goldman, and P. Gaspard, Topological hofstadter insulators in a two-dimensional quasicrystal, Physical Review B **91**, 085125 (2015).

[22] E. Prodan, Virtual topological insulators with real quantized physics, Physical Review B **91**, 245104 (2015).

[23] L. Morini and M. Gei, Waves in one-dimensional quasicrystalline structures: dynamical trace mapping, scaling and self-similarity of the spectrum, Journal of the Mechanics and Physics of Solids **119**, 83 (2018).

[24] M. Gei, Wave propagation in quasiperiodic structures: stop/pass band distribution and prestress effects, International Journal of Solids and Structures **47**, 3067 (2010).

[25] D. J. Apigo, K. Qian, C. Prodan, and E. Prodan, Topological edge modes by smart patterning, Physical Review Materials **2**, 124203 (2018).

[26] D. J. Apigo, W. Cheng, K. F. Dobiszewski, E. Prodan, and C. Prodan, Observation of topological edge modes in a quasiperiodic acoustic waveguide, Physical Review Letters **122**, 095501 (2019).

[27] X. Ni, K. Chen, M. Weiner, D. J. Apigo, C. Prodan, A. Alù, E. Prodan, and A. B. Khanikaev, Observation of hofstadter butterfly and topological edge states in reconfigurable quasi-periodic acoustic crystals, Communications Physics **2**, 55 (2019).

[28] R. K. Pal, M. I. Rosa, and M. Ruzzene, Topological bands and localized vibration modes in quasiperiodic beams, arXiv preprint arXiv:1906.00151 (2019).

[29] D. R. Hofstadter, Energy levels and wave functions of bloch electrons in rational and irrational magnetic fields, Physical Review B **14**, 2239 (1976).